



Exploring thermal annealing and graphene-carbon nanotube additives to enhance crystallinity, thermal, electrical and tensile properties of aged poly(lactic) acid-based filament for 3D printing

Rumiana Kotsilkova^{a,*}, Ivanka Petrova-Doycheva^a, Dzhihan Menseidov^a, Evgeni Ivanov^{a,b}, Alesya Paddubskaya^c, Polina Kuzhir^c

^a OLEM, Institute of Mechanics, Bulgarian Academy of Sciences, Acad. G. Bonchev, Bl. 4, 1113, Sofia, Bulgaria

^b Research and Development of Nanomaterials and Nanotechnologies, NanoTechLab Ltd., Sofia, Bulgaria

^c Institute for Nuclear Problems, Belarusian State University, Bobruiskaya 11, 220030, Minsk, Belarus

ARTICLE INFO

Keywords:

Annealing
Raman spectroscopy
Differential scanning calorimetry (DSC)
Thermogravimetric analysis
Electrical properties
Mechanical properties

ABSTRACT

The shelf life performance of polylactic acid (PLA) filaments for 3D printing is limited by aging mechanisms in terms of durability. In this work, the aged PLA and composite filaments filled with 12 wt% of graphene nanoplatelets (GNP), multiwall carbon nanotubes (MWCNT), and their hybrid mixture (1:1) were studied, after 24 months storage in a laboratory environment. Solid annealing at 80 °C for 4 h and pre-melt annealing at 120 °C for 3 h were applied in order to improve the performances of the aged filaments. It was found that the graphene-carbon nanotube fillers enhance the crystallinity, thermal stability, electrical conductivity and tensile Young's modulus, along with reduced tensile strength, elongation and toughness, compared to the neat PLA. The annealing was found efficient to substantially improve mechanical, thermal and electrical properties of the aged PLA-based composite filaments however, the annealing temperature have to be tuned according to the type of carbon nanofiller and the target properties.

1. Introduction

Among biopolymers, poly(lactic acid) (PLA) gained much attention in additive manufacturing by fused deposition modeling (FDM), because of its easy printability, relatively good mechanical properties and biodegradability [1]. In the last years, an effective way was used to improve the properties of PLA by incorporating carbon-based nanomaterials that offer several unique features, such as electrical conductivity, thermal stability and mechanical reinforcement [2]. The performance of the PLA-based composites is limited in terms of durability, thus graphite nanoplatelets (GNPs) and carbon nanotubes (CNTs) are studied recently to add new physical properties to the PLA and to slow down its mechanical performance during biodegradation [3,4]. The only commercial graphene-enhanced filament with electrical conductivity and electromagnetic properties that is currently available on market is offered by Graphene Supermarket [5]. However, sitting of the filament in a place for 1 year or more, even in packaged conditions is not recommended by the producer as it causes deterioration of its properties.

The performance of the biodegradable PLA polymer in terms of

durability is limited by complex aging mechanisms including thermal degradation, hydrolysis, oxidation and natural weathering [4]. The thermal and UV light degradation of PLA is accompanied by a significant decrease in crystallinity and the reduction of mechanical properties, which was associated with the PLA chain scission and formation of surface cracks [6,7]. At realistic in-service environments, the degradation rate of PLA parts is found slow and the hydrolysis aging can be neglected in air [7]. Therefore, the control and manipulation of physical and mechanical properties of PLA-based filaments during aging in air is the key for variety of long lasting successful applications of both filaments and 3D printed parts.

Another weak point for the PLA-based filaments is that their mechanical properties depend strongly on the processing conditions, which influence the PLA crystallinity [8]. Mechanical properties of PLA polymers can be varied from soft-and-elastic plastics to stiff-and-high strength materials depending on crystallinity. Nano sized additives in PLA polymer are reported to influence the crystalline kinetics and morphology, so they can be used as a tool for tuning specific physical and mechanical properties by providing nucleation agents to initiate crystallization [9]. The materials with higher crystallinity show

* Corresponding author.

E-mail address: kotsilkova@imb.bas.bg (R. Kotsilkova).

<https://doi.org/10.1016/j.compscitech.2019.107712>

Received 11 May 2019; Received in revised form 23 June 2019; Accepted 30 June 2019

Available online 02 July 2019

0266-3538/ © 2019 Elsevier Ltd. All rights reserved.

increased mechanical properties and are thought to have improved durability. Enhanced nucleation rate of polylactide assisted by addition of carbon nanotubes is widely reported [10]. Recently, Wu et al. [11] observed that the cold and melt crystallization behaviors of PLA depend strongly on the presence of graphene nanoplatelets. During cold crystallization, GNPs act as inert filler, but during melt crystallization, the GNPs dominantly act as heterogeneous nucleating agent and increase the crystallization rate compared to the neat PLA. The crystallinity began to decrease at higher cooling rates and higher GNP content, due to the slowly crystallizing PLA polymer and the GNPs aggregation [12]. Li et al. [13] performed a comparative crystallization study on PLA composites with CNTs and GNPs. Both nanofillers are found to serve as heterogeneous nucleation agents, however, the induction ability of CNTs is stronger than that of GNPs, due to the multiple orientations of PLA lamellae on the large two-dimensional flat area of GNPs, which suppressed the crystal growth.

Annealing on PLA polymer was reported to be an efficient treatment to increase modulus, tensile strength and reduce gas permeability, because of increased crystallinity. Variety of time-temperature conditions were applied for annealing of PLA and different effects are reported [14–16]. Thus, the crystallinity and melting temperature of PLA are found to increase with increasing the annealing temperature in the range 100–140 °C. The filler loading in conjunction with annealing may affect significantly the melting behavior, glass transition temperature, crystallinity and mechanical properties of PLA. Authors found, that the addition of clay, wood flour, cellulose and basalt fibers, combined with annealing lead to higher crystallinity and enhanced Young modulus, impact strength, flexural modulus and stiffness, but their flexural strength decreased [17–19]. Systematic effects on electrical conductivity of carbon nanotube filled polymers were observed as a function of annealing temperature and time, and this relationship was related to reorientation of nanotubes due to enhanced polymer mobility [20–23]. Moreover, electrical conductivity of hybrid nanocomposites incorporating small and large GNP fillers was found greatly improved by pre-melt annealing at elevated temperatures [23]. Such phenomenon was named “dynamic percolation”, as opposed to traditional statistical percolation [22].

In our previous study [24] we have compared the fresh and aged composites based on PLA with 6 wt% graphene and carbon nanotubes produced by solution blending and extrusion. The efficiency of solid annealing and reprocessing for the recovery of aged nanocomposite films were investigated by surface mechanical tests. There is a need for further research in this area, as it is important to understand how efficient will be the combination of different annealing conditions and graphene-carbon nanotube additives in respect to improving the multifunctionality of aged PLA-based filaments. In the present study, we investigate the crystallinity, thermal, electrical and tensile properties of the aged for 24 months PLA-based filaments filled with 12 wt% graphene, carbon nanotubes and their hybrid mixture (1:1). The highly filled filaments were produced in our Labs aiming to achieve good mechanical properties, combined with superior conductivity and electromagnetic efficiency. The effects of solid annealing at 80 °C for 4 h and pre-melt annealing at 120 °C for 3 h on the properties of the aged composite filaments were studied. The final goal is to propose an effective way for improving electrical, mechanical and thermal performance of highly filled PLA-graphene-carbon nanotube filaments for 3D printing, after long time storage, above the shelf life.

2. Materials and methods

2.1. Materials

The poly (lactic) acid polymer (PLA) Ingeo™ Biopolymer PLA-3D850 (Nature Works) with MFR 7–9 g/10 min (210 °C, 2.16 kg) was used as a matrix polymer. Graphene nanoplatelets (GNPs) with purity 90 wt%; median size 5–7 µm, with size polydispersity 0.5–25 µm; number of

graphene layers < 30, as well as –OH functionalized multiwall carbon nanotubes (MWCNTs) having purity 95 wt%, –OH content 2.48%, outer diameter 30 nm, inner diameter 5–10 nm, length > 10 µm, aspect ratio ~ 1000, were supplied from TimesNano, China.

Twin-screw extruder (COLLIN Teach-Line ZK25T) was used to prepare nanocomposite pellets by melt extrusion of PLA and filler in appropriate amounts at temperatures 170–180 °C and screw speed 40 rpm. The nanocomposite pellets were further extruded to filaments with 1.75 mm diameter by single screw extruder (Friend Machinery Co.) at 10 rpm within temperatures 170–180 °C followed by quenching in water bath at 60 °C. Monofiller composite filaments containing 12 wt% GNP and MWCNTs, as well as a bifiller filament with 6 wt% GNP/6 wt% MWCNT in PLA were produced for this study. The difference in size, shape and connectivity between the large graphene nanoplatelets and the curved MWCNTs in their powder form, as well as the production of filaments were published elsewhere [25].

The produced filaments were stored in laboratory environment for 24 months at ambient temperature 25 °C and humidity 60–70%. Two time-temperature conditions were applied for annealing of the aged filaments: (i) solid annealing at 80 °C for 4 h (above the glass transition); and (ii) pre-melt annealing at 120 °C for 3 h (above the cold crystallization and before melting). The aged non-annealed filaments were tested as “control” samples. Table 1 summarizes the filament samples and the annealing conditions.

2.2. Experimental methods

Raman spectroscopy analysis was performed for the nanofillers and the nanocomposites using Raman spectrometer Nanofinder High End (Tokyo Instruments) combined with a confocal microscope and 473 nm laser excitation. Raman spectra were collected using 100x objective and the exposition time was set to 30 s. To decrease sample degradation, the average laser power did not exceed 1 mW.

Differential scanning calorimeter DSC-Q20 (TA Instruments) was used to monitor the heat effects associated with phase transitions of the polymer as a function of temperature. Samples underwent a heating/cooling in the temperature range from 30 to 200 °C at 20 °C/min in a nitrogen atmosphere with gas flow rate of 50 mL/min. From the DSC thermograms the glass transition (T_g), cold crystallization (T_{cc}), melting peak (T_m), melt crystallization temperature (T_c), exothermic cold crystallization enthalpy (ΔH_{cc}), endothermic melting enthalpy (ΔH_m) and degree of crystallinity (χ_c) were evaluated. Taking into account that the PLA undergoes cold crystallization during heating, the degree of crystallinity of PLA was calculated from Eq. (1):

$$\% \text{ crystallinity } (\chi_c) = \left(\frac{\Delta H_m - \Delta H_{cc}}{w \Delta H_m^0} \right) * 100 (\%) \quad (1)$$

where: ΔH_m is fusion/melting enthalpy (J/g), ΔH_{cc} is the cold crystallization enthalpy (J/g), and ΔH_m^0 (93 J/g) is the melting enthalpy when the crystallinity of PLA is 100% [26]. Enthalpy values for nanocomposites were normalized on the actual amount of polymer (w) involved in the thermal transition, as the filler is not involved in melting/crystallization processes. This approximate equation can provide

Table 1
Aged filaments for 24 months and annealing conditions used in this study.

Aged Filament	Composite acronym	Filler content, wt%
Neat PLA	PLA	0
12 wt% GNP/PLA	12GNP/PLA	12
12 wt% MWCNT/PLA	12CNT/PLA	12
6 wt% GNP/6 wt% MWCNT/PLA	6GNP/6CNT/PLA	12
Annealing Conditions	Temperature, [°C]	Time
Control (non-annealed)	25 °C	24 Months aging
Solid annealing	80 °C	4 h
Pre-melt annealing	120 °C	3 h

information on the crystallinity of the sample removing the effects due to cold crystallization and filler content.

Thermal gravimetric analysis (TGA) was conducted using a TG/DTA-Q50 (TA Instruments) at 10 °C/min from 30 to 400 °C in a nitrogen atmosphere with gas flow rate of 50 mL/min. The samples (ca. 10 mg) were placed in open platinum pans. The decomposition steps and characteristic temperatures, such as onset of thermal decomposition (T_{onset}), temperature at 10% weight loss ($T_{10\%}$) and peak of degradation (T_{peak}) were determined from the TG and DTG curves, respectively.

The electrical conductivity was measured via volt-ampere (V-A) circuit, using the High Resistance Electrometer Keithley 6517b (Beaverton, OR, USA). The test samples were filaments of 50 mm length and 1.75 mm diameter. The samples were metalized in four sections, each of length 5 mm followed by 10 mm non-metalized sections in between. The test was conducted at room temperature of about 20 °C with direct reading of the flushing current between two adjacent metallized zones. Three measurements were made at different places of each sample, as well as three samples of each composition were tested. A classical formula was used to calculate the electrical conductivity depending on the resistivity of material, $\sigma = \frac{L}{R\pi r^2}$ [S/m], where: R – electrical resistivity, L – sample length, and r – radius of the cross section of the sample.

Tensile mechanical measurements were carried out using Universal Mechanical Testing Machine (UMT-2, Bruker). The test specimens were filaments with circular cross-section of diameter 1.75 mm and length 50 mm. Tensile test was performed at room temperature by using 1 kN sensor, with a tensile speed of 1 mm/min. The standard error was determined by testing of 7–10 samples of each composition. Tensile mechanical characteristics determined from the test were, namely: Young's modulus, yield strength, ultimate strength, elongation at ultimate strength and toughness.

3. Results and discussion

3.1. Raman characteristics of fillers and composites

The optical images of the bifiller MWCNT/GNP/PLA composite surface are presented in Fig. 1 (a,b). The blue spots indicate the point where the Raman spectra are collected. The Raman spectra of the fillers, GNP and MWCNT, as well as their PLA-based monofiller and bifiller composites are presented on Fig. 1 (c, d). All spectra are normalized for the intensity of G band. As seen, the spectra of the carbon nanomaterials are dominated by several strongest features: the high-frequency G band ($\sim 1580 \text{ cm}^{-1}$) originates from in-plane vibrations of sp^2 -hybridized carbon-atoms, the D band ($\sim 1360 \text{ cm}^{-1}$) occurs due to disorder-induced symmetry-lowering effects and often this band is used as an indicator of the presence of defects in the carbon lattice. The 2D band ($\sim 2700 \text{ cm}^{-1}$) arises from the two-phonon, second-order scattering process, and it is highly sensitive to the number of graphene layers [27]. Similar to bulk graphite, due to multilayer structure, the GNPs spectrum of initial powder (in Fig. 1(c)) consists of a very broad (full-width-half-maximum (FWHM) $\sim 80 \text{ cm}^{-1}$) and asymmetric 2D peak which has a relative intensity 3 times smaller than the intensity of G band. The small ratio of the intensity of G and D bands ($I_D/I_G \sim 0.13$) indicates the high crystalline quality of GNPs. On the contrary (in Fig. 1(d)), the same ratio I_D/I_G is larger in the case of MWCNTs ($I_D/I_G \sim 0.57$) which can be associated with the high degree of structural disorder of this material and more defects due probably to the presence of –OH functional groups on the MWCNT surfaces.

For the composite samples, the relative intensity of D band increases, which indicates for a small degradation of carbon nanomaterials during composite processing. In Fig. 1(c), the spectra of GNP/PLA composite are similar to that of GNP filler. The low intensity D band, as well as more intense and sharper 2D band pointed in the spectra of GNPs and GNP/PLA indicates for few layers graphene. Similar low

values of I_{2D}/I_G ratios (0.158–0.193) for both GNP powder and GNP/PLA composite demonstrate that the graphene layers are not exfoliated in the PLA. In contrast, in Fig. 1 (d) the Raman spectra of MWCNT/PLA composites, similar to the spectra of MWCNT filler, showed an intense D band and intense 2D band, due to the few graphite layers in the multi-walled carbon nanotube structure. However, all Raman bands for the monofiller and bifiller composites in Fig. 1(d) related to the MWCNTs are shifted to higher wavenumber (for example, G-band shifts from 1575 cm^{-1} in initial powder up to 1587 cm^{-1} in composite). Such effect may be attributed to a disentanglement of MWCNTs and decreasing inter-tube interaction in the polymer matrix [28]. The disentangled MWCNTs obviously provides more surfaces for interaction with the polymer molecules. This was confirmed by the weak blue shift of the G band in the monofiller CNT/PLA and bifiller GNP/CNT/PLA composites, which could be understood in terms of the strain effect caused by interfacial interaction between carbon nanotubes and PLA matrix [29]. However, the collected Raman spectra for the bifiller composites is very sensitive to the selected point on the sample's surface, e.g. near or far from the respective carbon nanoparticles, as seen in optical images, Fig. 1(a and b) and corresponding spectra, Fig. 1 (c,d).

3.2. Effects of annealing and graphene-carbon nanotube additives on PLA crystallinity and thermal properties

3.2.1. Cold crystallization and melting during heating

In order to study the effect of thermal history and annealing, the 'as received' aged filaments were characterized by the DSC thermograms (results from the first heating run), followed by subsequent cooling. In Fig. 2, the DSC curves of heat flow vs. temperature are presented, where the first column graphs compare the 1st heating run and the second column graphs show the subsequent cooling after 1st heating run, comparing the non-annealed and annealed filaments. Thermal characteristics are summarized in Table 2.

In Fig. 2(a and b), the DSC thermograms of the non-annealed filaments are presented, as a control. The 12 wt% filled composite filaments demonstrate several typical thermal events during heating, such as glass transition (T_g), cold crystallization (T_{cc}), crystalline phase transition peak (T_{cc1}) and melting (T_m), as well as a melt crystallization (T_c) during cooling. In contrast, only glass transition and a small melting peak were evident for the neat PLA filament during heating. The absence of crystallization peak and the small melting peak for the neat PLA filament indicate that the homopolymer is difficult to be crystallized from glassy state. However, by addition of GNPs and MWCNTs, a cold crystallization (at $T_{cc} \sim 100 \text{ °C}$) and the crystalline phase transition from crystal form α to α' (at $T_{cc1} \sim 162 \text{ °C}$) are induced [30,31]. Obviously, both carbon nanofillers favored the crystallization of the PLA from glassy state, but the effect of MWCNTs is stronger, as pointed by the $\sim 4 \text{ °C}$ lower T_{cc} compared to the composites containing GNPs.

Importantly, the melting temperature (T_m) of the composite filaments is shifted up with 26 °C to higher temperatures ($\sim 176 \text{ °C}$) compared to the neat PLA ($\sim 150 \text{ °C}$), which is associated with melting of large portion of crystals in composites, which are formed due to the nucleation effect of GNPs and MWCNTs.

In contrast, the annealing dramatically changed the thermal behavior of the neat PLA and the composites during heating, as seen in Fig. 2 (c,e). However, the effects of the solid and pre-melt annealing on the DSC 1st heating thermograms are similar. The T_g of the composite filaments is with $\sim 5 \text{ °C}$ higher than that of the neat PLA, due to the suppressed chain relaxation and the reduced mobility because of presence of nanofillers. The cold crystallization peak is disappeared in the annealed composites showing that the annealing has a hindrance role rather than a nucleating during cold crystallization of PLA. The crystalline phase transition peak is observed at the same temperature, $T_{cc1} \sim 162 \text{ °C}$, as for the control sample, thus it is not affected by the annealing conditions and the type of carbon filler, [15,31]. While, the

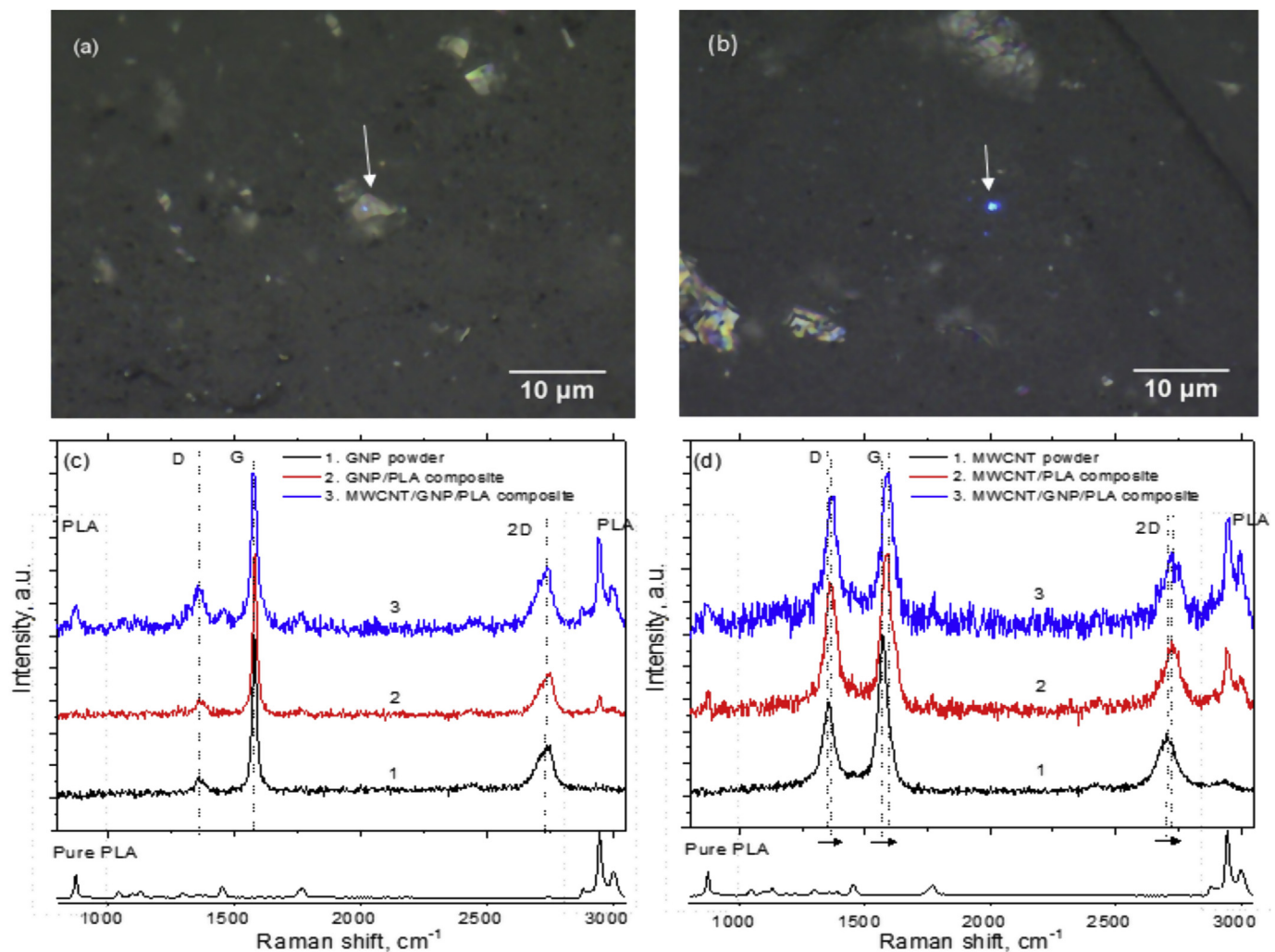


Fig. 1. Raman spectra of the filaments and fillers: (a,b) Optical images of the bifiller composite filaments: arrows indicate the points where the Raman spectra were collected: (a) GNP particle (left) and (b) MWCNTs (right); (c,d) Raman spectra of carbon nanoparticles in the initial powder and in the polymer composites: (c) GNPs; (d) MWCNTs. Below is the PLA spectrum.

annealed neat PLA show well-presented two overlapped melting peaks (T_{m1} and T_m), due to the slow rate of crystallization and the reorganization of crystalline phase in PLA during annealing [32], which are not presented in the annealed composite filaments, due to the nucleation effects of GNPs and MWCNTs.

The melting temperature (T_m) of annealed composites is kept of $\sim 26^\circ\text{C}$ higher value than that of the annealed neat PLA. The heat capacity, associated with the glass transition (T_g) is observed higher for the non-annealed filaments, while this heat is very small for the annealed filaments, due to the absorbed moisture in the aged samples, which was evaporated during annealing.

3.2.2. Degree of crystallinity and melt crystallization behavior

The crystallinity was determined by DSC 1st heating run (Fig. 2 a,c,e) from the enthalpies of cold crystallization and melting (ΔH_{cc} and ΔH_m). The degree of crystallinity (χ_c , %) was calculated by Eq. (1) and the results are summarized in Table 2. As seen, the non-annealed neat PLA filament is almost amorphous material ($\chi_c = 1.6\%$). Both graphene and carbon nanotube additives increase the crystallinity of PLA in the non-annealed composites to 17–21%, due obviously to heterogeneous nucleation [12], where the nucleation effect of MWCNTs is slightly stronger than that of GNPs. Importantly, the annealing enhanced strongly the degree of crystallinity to 24–36% for the neat PLA and to 48–49% for the composites. If compare the effects of annealing

conditions, it may be concluded that there is not a significant difference in the degree of crystallinity of the aged composite filaments subjected to the solid annealing at 80°C for 4 h and the pre-melt annealing at 120°C for 3 h. For the neat PLA, however, the pre-melt annealing produced the highest crystallinity level compared to the solid annealing. The highly increased crystallinity of the composite filaments by annealing is expected to enhance their mechanical properties, due to the additional nucleation effect of graphene-carbon nanotube additives, producing reinforcement.

The effect of carbon-based additives and annealing on the melt crystallization was investigated during cooling after first heating run, in Fig. 2 (b, d, f). The neat PLA filament did not show melt crystallization before and after annealing, suggesting that the homopolymer used in this work is hard to be crystallized from molten state in the non-isothermal quenching process. However, the composite filaments demonstrate intensive melt crystallization with peak temperatures (T_c) strongly depending on the type of carbon filler. The highest onset and the peak of melt crystallization was observed for the GNP/PLA composite ($T_c \sim 110^\circ\text{C}$), followed by the bi-filler GNP/MWCNT/PLA composite ($T_c \sim 108^\circ\text{C}$), while the lowest melt crystallization peak ($T_c \sim 105^\circ\text{C}$) was observed for the MWCNT/PLA composite. This confirms Ref. [11,13] that the presence of GNPs has stronger influence on the melt crystallizations of PLA due to heterogeneous nucleating effect, than the MWCNTs. This process is opposite to the cold crystallization

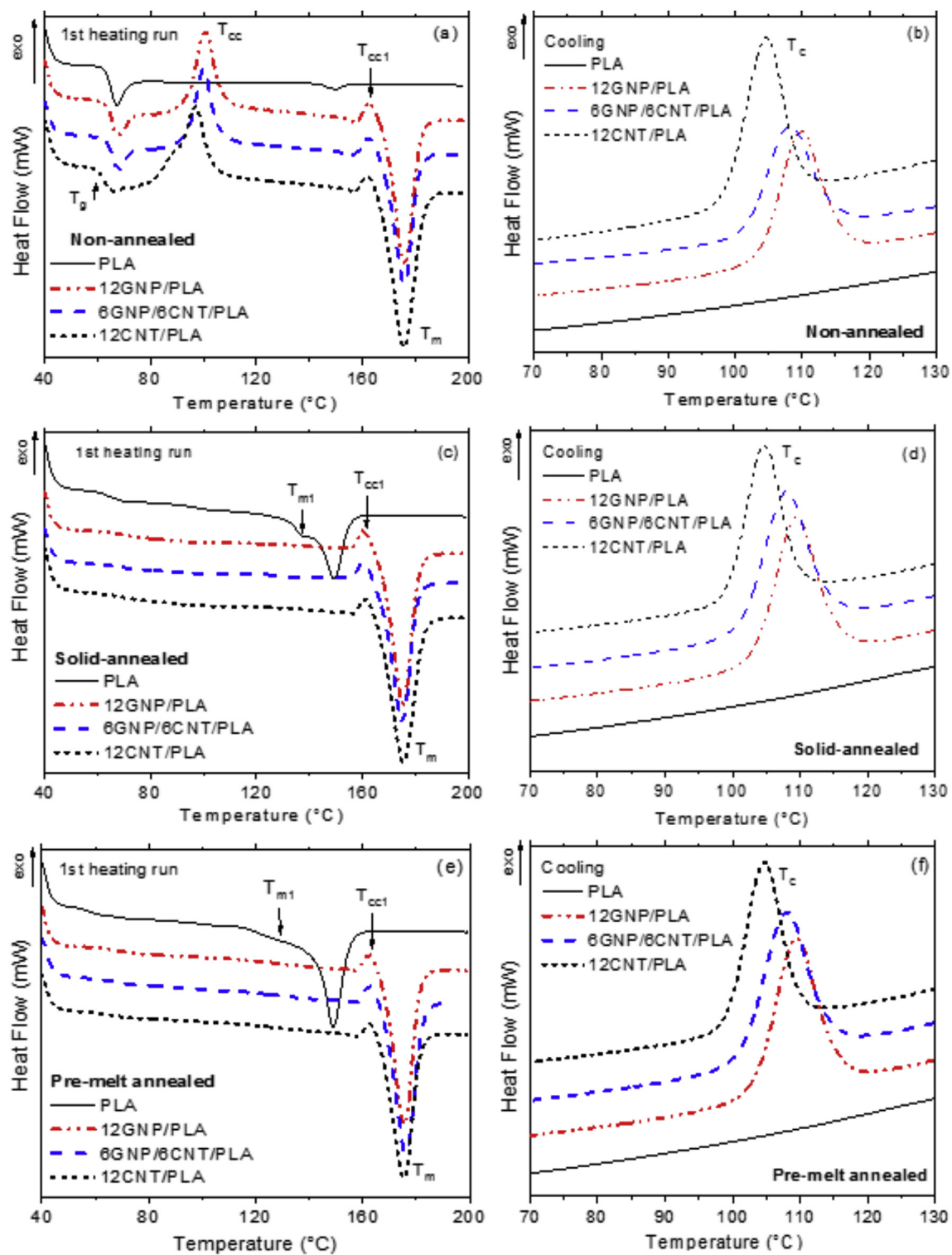


Fig. 2. DSC thermograms, first heating run (first column graphs) and subsequent cooling (second column graphs) of the aged filaments: (a,b) control (non-annealed) filaments; (c,d) solid annealed filaments at 80 °C for 4 h; (e,f) pre-melt annealed one at 120 °C for 3 h.

process, in the DSC 1st heating run (Fig. 2 a,c,d), where the presence of MWCNTs favours in larger extent the cold crystallization of PLA than the CNPs.

3.2.3. Thermal stability and degradation

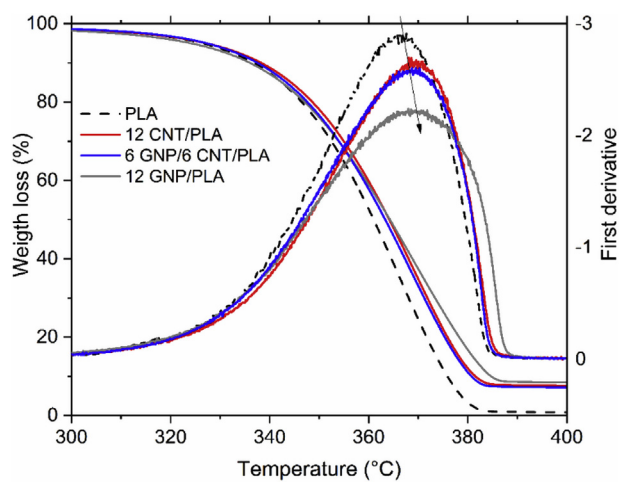
The TGA curves in Fig. 3, present the relative weight loss and the corresponding first derivative (DTG) vs. temperature of the aged filaments, containing 12 wt% GNPs, MWCNTs and mixed fillers (1:1),

compared with the neat PLA filament. In Table 3, the characteristic decomposition temperatures, such as: the onset of degradation (T_{onset}), the temperature at 10% weight loss ($T_{10\%}$) and the DTG peak of degradation (T_p) are summarized. The weight loss (%) at T_{onset} is presented in order to estimate the absorbed moisture in the aged filaments. As seen in Fig. 3, the nanocomposites degraded with a single step corresponding to the thermal degradation of the PLA polymer, this initiated primarily by thermal scissions of C–C chain bonds [32]. The

Table 2

Thermal characteristics determined by DSC first heating run and subsequent cooling.

Status	Composites	T _g [°C]	T _{cc} [°C]	T _{cc1} [°C]	T _{m1} [°C]	T _m [°C]	T _c [°C]	ΔH _{cc} [J/g]	ΔH _m [J/g]	χ _c [%]
Non annealed Control	PLA	65.0	–	–	–	149.6	–	–	1.47	1.6
	12GNP/PLA	65.5	100.7	162.0	–	175.9	109.8	22.6	36.9	17.4
	12CNT/PLA	62.5	96.8	161.8	–	175.6	104.6	21.8	38.6	20.5
	6GNP/6CNT	65.6	100.1	162.0	–	175.7	108.1	22.7	37.6	18.2
Solid annealed	PLA	64.0	–	–	127.3	149.3	–	–	22.3	24.0
	12GNP/PLA	69.9	–	160.4	–	175.3	109.2	–	39.9	48.8
	12CNT/PLA	70.2	–	160.9	–	175.4	104.5	–	40.3	49.2
	6GNP/6CNT	68.6	–	160.3	–	174.9	108.4	–	39.7	48.5
Pre-melt annealed	PLA	58.0	–	–	127.7	149.0	–	–	33.6	36.1
	12GNP/PLA	66.1	–	162.3	–	175.5	109.4	–	38.8	47.4
	12CNT/PLA	64.0	–	162.2	–	175.3	104.6	–	38.9	47.5
	6GNP/6CNT	66.3	–	162.6	–	176.1	107.9	–	39.6	48.4

**Fig. 3.** TGA curves of weight loss vs. temperature and the corresponding first derivative (DTG curves) in nitrogen atmosphere. Data for aged PLA and nanocomposite filaments with 12 wt% GNPs, MWCNTs and mixed fillers.**Table 3**Characteristic decomposition temperatures of aged filaments, control and annealed (AC1): TGA onset (T_{onset}), TGA at 10% weight loss (T_{10%}) and DTG peak temperature (T_p).

Sample name		T _{onset} , °C	T _{10%} , °C	T _{peak} , °C	Weight Loss at T _{onset} , %
Control	PLA	230	337	365	0.65
	12GNP/PLA	248	338	372	0.73
	12CNT/PLA	242	336	368	0.71
	6GNP/6CNT/PLA	248	338	370	0.66
Solid annealed	PLA	233	335	371	0.36
	12GNP/PLA	249	340	375	0.26
	12CNT/PLA	245	336	374	0.27
	6GNP/6CNT/PLA	248	337	373	0.27

GNPs show the highest improvement of the thermal stability, as presented by T_{onset}, which is shifted up to higher temperatures with 18 °C for the composites with GNPs and with 12 °C for the composites with MWCNTs, if compared to that of the neat PLA (Table 3). This may be associated with the continuous platelet structure of GNPs, that facilitate the heat transfer suppressing the initial polymer degradation, due to the high thermal conductivity of carbon filler.

However, the high temperature processes of thermal degradation above 335 °C, such as the T_{10%} and T_p are slightly shifted by 2–5 °C to higher temperatures, compared to the neat PLA which confirm the upper suggestion. The broader DTG peak with lower intensity for the 12GNP/PLA composite compared to the neat PLA could be attributed to

the barrier labyrinth effect of graphene nanoplatelets, so that the heat transfer and the diffusion of degradation products from the bulk of the polymer to the gas phase is slowed down by the GNPs.

As seen from Table 3, the solid annealing has insufficient effect on the thermal stability and degradation of PLA-based composite filaments. Similar behavior was observed for the pre-melt annealed filaments (not presented here). However, if compare the weight loss (%) at the T_{onset} before and after annealing, one may see approximately twice higher mass loss (~0.7 wt%) for the control (non-annealed) filament compared to the annealed one (~0.3 wt%). This may be associated with the absorbed moisture in the aged non-annealed filaments during storage that is removed by annealing.

3.3. Effects of annealing on electrical conductivity of composite filaments

The effects of carbon fillers, the solid and the pre-melt annealing on the electrical conductivity of the composite filaments, containing 12 wt % GNPs, MWCNTs and mixed filler (1:1) were presented in Fig. 4. Data are summarized in Table 4. The three studied filaments are conductive, as the filler content is highly above the statistical percolation, which is around 1.5 wt% for MWCNT/PLA, 6 wt% for GNP/PLA and 3 wt% for MWCNT/GNP/PLA composites, as determined in our previous studies [25,33]. However, the non-annealed 12 MWCNT/PLA filament demonstrated 7-folds higher electrical conductivity, compared to the 12GNP/PLA, due obviously to the better dispersion of MWCNTs in the PLA matrix, compared to that of GNPs, as found from the Raman spectra in Fig. 1. While the bifiller composite filament 6MWCNT/6GNP has electrical conductivity, similar to that of the monofiller composite filament containing only graphene (Table 4).

The solid annealing performed at 80 °C for 4 h (i.e. above the glass transition temperature, T_g ~ 65 °C), resulted in an insufficient effect or even slightly reducing the electrical conductivity of the three highly

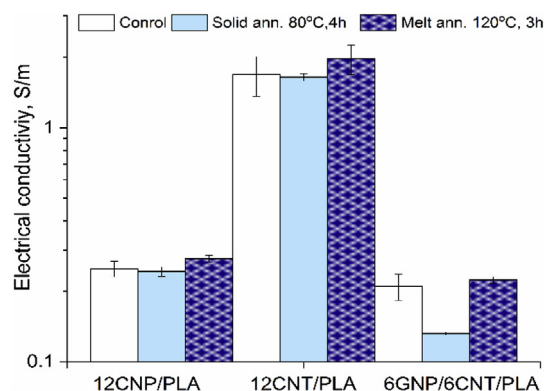
**Fig. 4.** Electrical conductivity of composite filaments: 12GNP/PLA, 12 MWCNT/PLA and 6GNP/6MWCNT/PLA. Comparison of non-annealed, solid annealed and pre-melt annealed filaments.

Table 4
Electrical conductivity of the composite filaments before and after annealing.

Filament Type	Electrical conductivity, S/m			
	Control non-annealed	Solid annealed 80 °C, 4 h	Pre-melt annealed 120 °C, 3 h	% increase
12GNP/PLA	0.250 ± 0.019	0.243 ± 0.011	0.276 ± 0.009	11%
12CNT/PLA	1.684 ± 0.324	1.643 ± 0.060	1.973 ± 0.284	17%
6GNP/6CNT/PLA	0.210 ± 0.027	0.132 ± 0.002	0.224 ± 0.007	7%

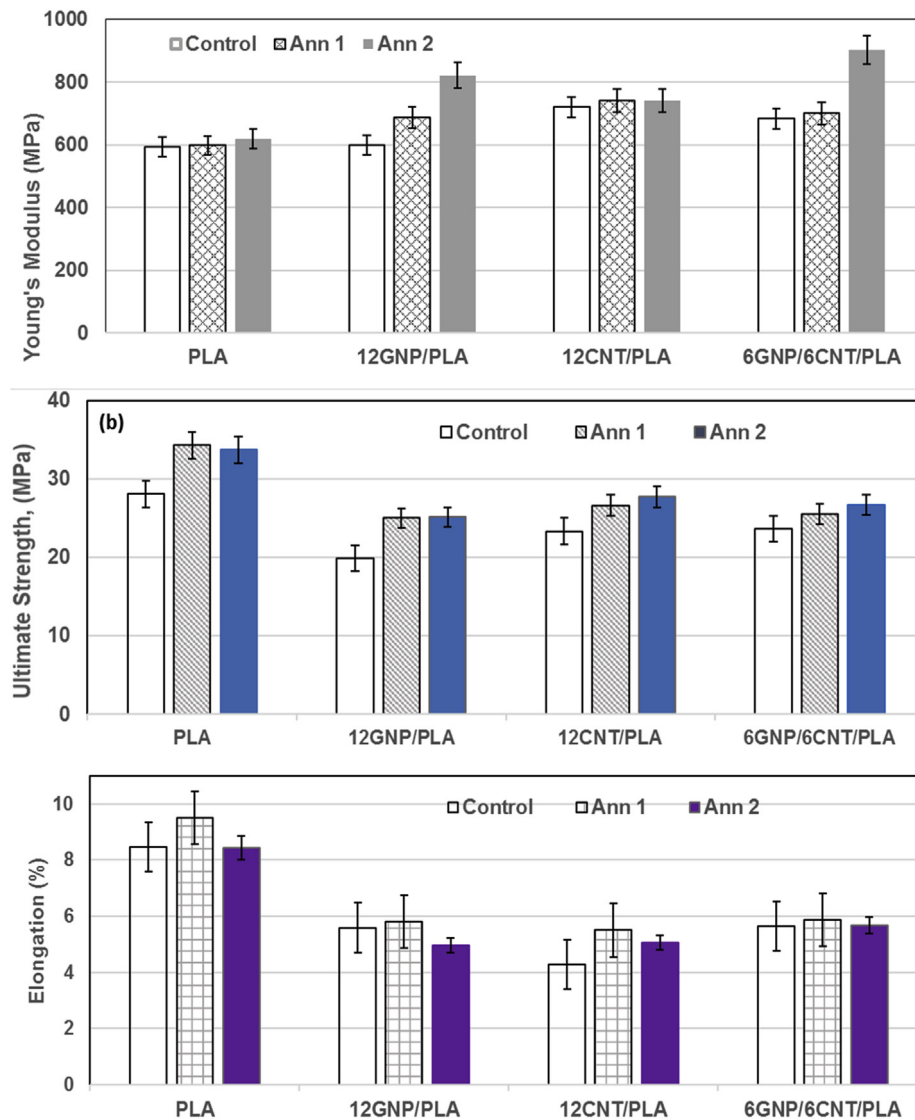


Fig. 5. Effect of solid annealing at 80 °C and pre-melt annealing at 120 °C on the tensile characteristics: (a) Yong's modulus, (b) ultimate strength, (c) elongation at ultimate strength, of aged PLA and composite filaments. Non-annealed filaments (empty bars), solid annealed (pattern bars) and pre-melt annealed (full bars) filaments.

filled composite filaments. In contrast, the pre-melt annealing at 120 °C for 3 h (i.e. above the cold crystallization temperature, $T_{cc} \sim 100$ °C) resulted in a moderate increase of electrical conductivity (of 7–17%), depending on the type of nanofiller. Researchers described such relationship as a dynamic percolation in highly oriented conductive networks formed by carbon nanofillers upon annealing [20–22]. However, our study shows that at the highly filled composites with 12 wt% carbon nanofillers, the increase of conductivity upon pre-melt annealing is not so high, due probably to the large amount of polymer attracted on the nanofiller surfaces, which suppressed the polymer mobility and reduced the dynamic percolation effect.

3.4. Tensile properties of aged filaments affected by annealing history and graphene-carbon nanotube additives

Series of tests were performed to evaluate tensile mechanical characteristics of aged filaments, such as Young's modulus, tensile strength and elongation, yield strength and toughness. The effects of solid and pre-melt annealing, combined with the reinforcement effect of graphene-carbon nanotube additives on the tensile properties were evaluated and the results are summarized in Fig. 5 and Table 5.

Table 5

Tensile mechanical characteristics of aged PLA and composite filaments before and after annealing at two time-temperature conditions.

Composition	Annealing conditions	Young's Modulus (MPa)	Ultimate Strength (MPa)	Yield Strength (MPa)	Elongation (%)	Toughness (J/mm ³)
PLA	Control	593.6 ± 8.5	28.1 ± 3.9	6.22 ± 0.9	8.45 ± 1.6	1.16
	Ann 1, solid annealing	98.9 ± 6.5	34.3 ± 1.5	6.55 ± 0.8	9.50 ± 0.6	1.63
	Ann 2, pre-melt annealing	619.6 ± 5.7	33.7 ± 1.2	6.20 ± 1.1	8.44 ± 1.4	1.43
12GNP/PLA	Control	598.1 ± 8.7	19.7 ± 3.3	4.63 ± 0.8	5.59 ± 0.7	0.56
	Ann1, solid annealing	687.5 ± 9.7	25.0 ± 1.2	5.09 ± 0.1	5.81 ± 0.2	0.73
	Ann 2, pre-melt annealing	820.9 ± 2.8	25.1 ± 1.3	3.09 ± 0.5	5.13 ± 0.8	0.63
12CNT/PLA	Control	719.9 ± 6.2	23.3 ± 1.9	3.36 ± 0.3	4.28 ± 0.4	0.51
	Ann 1, solid annealing	740.5 ± 9.1	26.6 ± 2.7	3.12 ± 0.2	5.50 ± 0.7	0.74
	Ann2, pre-melt annealing	712.9 ± 4.5	24.5 ± 2.1	2.07 ± 0.8	4.51 ± 1.4	0.54
6GNP/6CNT/PLA	Control	683.0 ± 4.2	23.7 ± 2.4	4.71 ± 0.6	5.63 ± 0.5	0.67
	Ann1, solid annealing	700.2 ± 4.1	25.5 ± 0.5	4.81 ± 0.2	5.86 ± 0.4	0.75
	Ann 2, pre-melt annealing	904.1 ± 4.3	26.7 ± 1.4	3.15 ± 0.5	5.51 ± 0.8	0.71

3.4.1. Effect of graphene-carbon nanotube additives on tensile properties of non-annealed filaments

If consider the non-annealed samples (the empty bars in each set of Fig. 5), one can see that the 12 wt% graphene-carbon nanotube additives in aged composite filaments strongly enhanced the Young's modulus and this effect is the highest in the monofiller and bifiller composites containing MWCNTs. Thus, 12CNT/PLA and 6GNP/6CNT/PLA show elastic modulus enhanced by 21% and 15%, respectively, compared to the neat PLA. While, the addition of GNPs has insufficient effect on the elastic modulus of non-annealed filaments. The improved tensile Young's modulus may be explained with much stronger nucleation effect of MWCNTs compared to the GNPs in the non-annealed composite filaments resulting in an increased rigidity.

In contrast, all other tensile characteristics, such as ultimate strength, yield strength, elongation and toughness are reduced for the composite filaments, compared to the neat PLA, due probably to high filler content of 12 wt%, which usually produced aggregation of nanofillers in the matrix PLA [34–36].

3.4.2. Effect of annealing history on tensile properties of aged filaments

The annealing resulted in a systematic improvement of the tensile characteristics of aged PLA and composite filaments, compared to the non-annealed one, particularly for Young's modulus, ultimate strength, and toughness. The results for yield strength and elongation are contradictory. However, different degree of improvements are observed depending on the annealing conditions and the type of carbon fillers.

If consider the Young's modulus (in Fig. 5(a)), the pre-melt annealing at 120 °C for 3 h produced strong improvement, ~37% for the 12 GNP/PLA and ~32% for the bi-filler composite, while this effect for the 12CNT/PLA composite is insufficient. Both pre-melt annealing and solid annealing improved the tensile strength (Fig. 5(b)) and toughness (Table 5) of the three composites filaments, however for toughness the degree of improvement produced by solid annealing is higher, compared to the pre-melt annealing. Elongation is increased by solid annealing with 4%–25%, depending on the type of the carbon filler, but the pre-melt annealing reduced slightly (2–9%) this characteristic. Toughness and elongation improvement by annealing is of crucial importance, as the PLA-based composite filaments are quite brittle materials, particularly the aged ones.

The differences in the improvement of tensile characteristics produced by the annealing history may be associated with different reorganization of the network of flat graphene nanoplatelets and disentangled MWCNTs, due the enhanced mobility of the polymer molecules during pre-melt annealing (at 120 °C) compared to the mobility produced by solid annealing (at 80 °C). At such high content of 12 wt% carbon nanofillers, large amount of polymer is attracted on the nanofiller surfaces, which obviously suppress the polymer mobility and reduce the dynamic percolation effect of the nanofiller. Moreover, the different degree of dispersion of both the disentangled MWCNTs and the aggregated GNPs in the matrix PLA definitely guarded the effect of

annealing on mechanical reinforcement.

4. Conclusions

In this study, the combined effects of annealing and graphene-carbon nanotube additives on thermal, electrical and tensile properties of aged for 24 months PLA-based filaments with high filler content of 12 wt% were investigated.

Both solid and pre-melt annealing strongly increased the % crystallinity of the aged PLA (24–36%) and the composite filaments (46–49%), this confirming the combined effect of nucleation and thermal treatment on the PLA crystallization. The enhanced crystallinity and different reorganization of the flat GNP platelets and disentangled MWCNTs in the matrix PLA obviously determinate the level of enhancement of Young's modulus, tensile strength, toughness and elongation by solid and pre-melt annealing.

The presence of 12 wt% GNPs shifted up with 18 °C the onset of thermal decomposition (T_{onset}), compared to the neat PLA, that is associated with the continuous platelet structure and high thermal conductivity of GNPs, which facilitate the heat transfer and suppress the initial polymer degradation. Importantly, the MWCNTs produces 7 folds higher conductivity than the GNPs, due probably to their better dispersion in the polymer. However, the pre-melt annealing produced a moderate increase (7–17%) of the electrical conductivity of the highly filled composites, while insufficient effect of annealing was observed on the thermal stability.

Obviously, the annealing temperature has to be tuned depending on the type of carbon nanofiller and the target characteristics for the highly filled PLA filaments with 12 wt% GNPs and MWCNTs.

Acknowledgements

This research was funded by the H2020-MSCA-RISE-2016-734164 Graphene 3D project. Authors R.K and E.I. acknowledge the support from the H2020-SGA-FET- GRAPHENE-785219 Graphene Core2 project.

Appendix A. Supplementary data

Supplementary data to this article can be found online at <https://doi.org/10.1016/j.compscitech.2019.107712>.

References

- [1] J.M. Raquez, Y. Habibi, M. Murariu, P. Dubois, Polylactide (PLA)-based nanocomposites, *Prog. Polym. Sci.* 38 (2013) 1504–1542 <https://doi.org/10.1016/j.progpolymsci.2013.05.014>.
- [2] C. Gonçalves, I.C. Gonçalves, F.D. Magalhães, A.M. Pinto, Poly(lactic acid) Composites Containing carbon-based nanomaterials: a review, *Polymers* 9 (269) (2017) 1–37, <https://doi.org/10.3390/polym9070269>.
- [3] T. Kuilla, S. Bhadra, D.H. Yao, N.H. Kim, S. Bose, J.H. Lee, Recent advances in graphene based polymer composites, *Prog. Polym. Sci.* 35 (2010) 1350–1375,

- <https://doi.org/10.1016/j.progpolymsci.2010.07.005>.
- [4] A.M. Pinto, C. Gonçalves, I.C. Gonçalves, F.D. Magalhães, Effect of biodegradation on thermo-mechanical properties and biocompatibility of poly(lactic acid)/graphene nanoplatelets composites, *Eur. Polym. J.* 85 (2016) 431–444, <https://doi.org/10.1016/j.eurpolymj.2016.10.046>.
 - [5] Graphene Supermarket, Conductive Graphene PLA Filament, (2009–2019) <https://graphene-supermarket.com/Graphene-Composites/> (accessed April 2019).
 - [6] M.S. Islam, K.L. Pickering, N.J. Foreman, Influence of accelerated ageing on the physico-mechanical properties of alkali-treated industrial hemp fibre reinforced poly(lactic acid) (PLA) composites, *Polym. Degrad. Stabil.* 95 (2010) 59–65, <https://doi.org/10.1016/j.polymdegradstab.2009.10.010>.
 - [7] D. Rasselet, A. Ruellan, A. Guinault, G. Miquelard-Garnier, C. Sollogoub, B. Fayolle, Oxidative degradation of polylactide (PLA) and its effects on physical and mechanical properties, *Eur. Polym. J.* 50 (2014) 109–116, <https://doi.org/10.1016/j.eurpolymj.2013.10.011>.
 - [8] A. Sodergard, M. Stolt, Properties of lactic acid based polymers and their correlation with composition, *Prog. Polym. Sci.* 27 (2002) 1123–1163, [https://doi.org/10.1016/S0079-6700\(02\)00012-6](https://doi.org/10.1016/S0079-6700(02)00012-6).
 - [9] A.M. Harris, E.C. Lee, Improving mechanical performance of injection molded PLA by controlling crystallinity, *J. Appl. Polym. Sci.* 107 (2008) 2246–2255, <https://doi.org/10.1002/app.27261>.
 - [10] Z. Xu, Y. Niu, Z. Wang, H. Li, L. Yang, J. Qiu, H. Wang, Enhanced nucleation rate of polylactide in composites assisted by surface acid oxidized carbon nanotubes of different aspect ratios, *ACS Appl. Mater. Interfaces* 3 (9) (2011) 3744–3753, <https://doi.org/10.1021/am200932q>.
 - [11] D. Wu, Y. Cheng, S. Feng, Z. Yao, M. Zhan, Crystallization behavior of polylactide/graphene composites, *Ind. Eng. Chem. Res.* 52 (20) (2013) 6731–6739, <https://doi.org/10.1021/ie4004199>.
 - [12] B. Yang, D. Wang, Ch Fang, S. Li-Fen, M. Ji-Bin, Ch Peng, Q. Jia-Sheng, X. Ru, L. Jing-Wang, Melting and crystallization behaviors of poly(lactic acid) modified with graphene acting as a nucleating agent, *J. Macromol. Sci. Part B* 58 (2) (2019) 290–304, <https://doi.org/10.1080/00222348.2018.1564222>.
 - [13] H.B. Li, M.A. Huneault, Effect of nucleation and plasticization on the crystallization of poly(lactic acid), *Polymer* 48 (2007) 6855–6866, [https://doi.org/10.1016/S1004-9541\(09\)60145-2](https://doi.org/10.1016/S1004-9541(09)60145-2).
 - [14] T. Tábi, I.E. Sajó, F. Szabó, A.S. Luyt, J.G. Kovács, Crystalline structure of annealed polylactic acid and its relation to processing, *Express Polym. Lett.* 4 (10) (2010) 659–668, <https://doi.org/10.3144/expresspolymlett.2010.80>.
 - [15] F. Carrasco, P. Pagès, J. Gámez-Pérez, O.O. Santana, M.L. MasPOCH, Processing of poly (lactic acid): characterization of chemical structure, thermal stability and mechanical properties, *Polym. Degrad. Stab.* 95 (2010) 116–125, <https://doi.org/10.1016/j.polymdegradstab.2009.11.045>.
 - [16] H. Tsuji, Y. Ikada, Properties and morphologies of poly(L-lactide): I. Annealing condition effects on properties and morphologies of poly(L-lactide), *Polymer* 36 (1995) 2709–2716, [https://doi.org/10.1016/0032-3861\(95\)93647-5](https://doi.org/10.1016/0032-3861(95)93647-5).
 - [17] A.A. Perez-Fonseca, J.R. Robledo-Ortiz, R. González-Núñez, D. Rodrigue, Effect of thermal annealing on the mechanical and thermal properties of polylactic acid–cellulosic fiber biocomposites, *J. Appl. Polym. Sci.* 133 (2017) (2016) 43750, <https://doi.org/10.1002/app.43750>.
 - [18] Z. Ying, D. Wu, M. Zhang, Y. Qiu, Polylactide/basalt fiber composites with tailorable mechanical properties: effect of surface treatment of fibers and annealing, *Compos. Struct.* 176 (2017) 1020–1027, <https://doi.org/10.1016/j.compstruct.2017.06.042>.
 - [19] M. Hrabalova, A. Gregorova, R. Wimmer, V. Sedlarik, M. Machovsky, N. Mundigler, Effect of wood flour loading and thermal annealing on viscoelastic properties of poly(lactic acid) composite films, *J. Appl. Polym. Sci.* 118 (2010) 1534–1540, <https://doi.org/10.1002/app.32509>.
 - [20] R. Zhang, A. Dowden, H. Deng, M. Baxendale, T. Peijs, Conductive network formation in the melt of carbon nanotube/thermoplastic polyurethane composite, *Compos. Sci. Technol.* 69 (2009) 1499–1504, <https://doi.org/10.1016/j.compscitech.2008.11.039>.
 - [21] B.H. Cipriano, A.K. Kota, A.L. Gershon, C.J. Laskowski, T. Kashiwagi, A.H. Bruck, Conductivity enhancement of carbon nanotube and nanofiber-based polymer nanocomposites by melt annealing, *Polymer* 49 (2008) 4846–4851, <https://doi.org/10.1016/j.polymer.2008.08.057>.
 - [22] S. Zhang, L. Lin, H. Deng, X. Gao, E. Bilotti, T. Peijs, Q. Zhang, Q. Fu, Dynamic percolation in highly oriented conductive networks formed with different carbon nanofillers, *Colloid Polym. Sci.* 290 (2012) 1393–1401, <https://doi.org/10.1007/s00396-012-2661-7>.
 - [23] Y. Gao, O.T. Picot, H. Zhang, E. Bilotti, T. Peijs, Synergistic effects of filler size on thermal annealing-induced percolation in polylactic acid (PLA)/graphite nanoplatelet (GNP) nanocomposites, *Nanocompos.* 3 (2) (2017) 67–75, <https://doi.org/10.1080/20550324.2017.1333780>.
 - [24] R. Kotsilkova, P. Angelova, T. Batakliov, V. Angelov, R. Di Maio, C. Silvestre, Study on aging and recover of poly (lactic) acid composite films with graphene and carbon nanotubes produced by solution blending and extrusion, *Coatings* 9 (6) (2019) 359, <https://doi.org/10.3390/coatings9060359>.
 - [25] G. Spinelli, P. Lamberti, V. Tucci, R. Ivanova, S. Tabakova, E. Ivanov, R. Kotsilkova, S. Cimmino, R. Di Maio, C. Silvestre, Rheological and electrical behaviour of nanocarbon/poly(lactic) acid for 3D printing applications, *Composites Part B* 167 (2019) 467–476, <https://doi.org/10.1016/j.compositesb.2019.03.021>.
 - [26] M. Pyda, R.C. Bopp, B.J. Wunderlich, Heat capacity of poly(lactic acid), *J. Chem. Thermodyn.* 36 (2004) 731–742, <https://doi.org/10.1016/j.jct.2004.05.003>.
 - [27] A.C. Ferrari, J.C. Meyer, V. Scardaci, C. Casiraghi, M. Lazzeri, F. Mauri, S. Piscanec, D. Jiang, K.S. Novoselov, S. Roth, A.K. Geim, Raman spectrum of graphene and graphene layers, *Phys. Rev. Lett.* 97 (2006) 18740, <https://doi.org/10.1103/PhysRevLett.97.18740>.
 - [28] L. Bokobza, J. Zhang, Raman spectroscopic characterization of multiwall carbon nanotubes and of composites, *Express Polym. Lett.* 6 (7) (2012) 601–608, <https://doi.org/10.3144/expresspolymlett.2012.63>.
 - [29] L.S. Schädler, S.C. Giannaris, P.M. Ajayan, Load transfer in carbon nanotube epoxy composites, *Appl. Phys. Lett.* 73 (1998) 3842, <https://doi.org/10.1063/1.122911>.
 - [30] J.M. Zhang, Y.X. Duan, H. Sato, H. Tsuji, I. Noda, S. Yan, Y. Ozaki, Crystal modifications and thermal behavior of poly(L-lactic acid) revealed by infrared spectroscopy, *Macromolecules* 38 (19) (2005) 8012–8021, <https://doi.org/10.1021/ma051232r>.
 - [31] Z. Liu, Y. Chen, W. Ding, C. Zhang, Filling behavior, morphology evolution and crystallization behavior of microinjection molded poly(lactic acid)/hydroxyapatite nanocomposites, *Composites Part A* 72 (2015) 85–95, <https://doi.org/10.1016/j.compositesa.2015.02.002>.
 - [32] A.J. Nijenhuis, E. Colstee, D.W. Grijpma, A.J. Pennings, High molecular weight poly (L-lactide) and poly(ethylene oxide) blends: thermal characterization and physical properties, *Polymer* 34 (1996) 5849–5857, [https://doi.org/10.1016/S0032-3861\(96\)00455-7](https://doi.org/10.1016/S0032-3861(96)00455-7).
 - [33] R. Kotsilkova, E. Ivanov, E. Krusteva, C. Silvestre, S. Cimmino, D. Duraccio, Isotactic polypropylene composites reinforced with multiwall carbon nanotubes, Part 2: thermal and mechanical properties related to the structure, *J. Appl. Polym. Sci.* 115 (2010) 3576–3585, <https://doi.org/10.1002/app.30413>.
 - [34] E. Ivanov, R. Kotsilkova, H. Xia, Y. Chen, R.K. Donato, K. Donato, A.P. Godoy, R. Di Maio, C. Silvestre, S. Cimmino, V. Angelov, PLA/Graphene/MWCNT composites with improved electrical and thermal properties suitable for FDM 3D printing applications, *Appl. Sci.* 9 (2019) 1209, <https://doi.org/10.3390/app9061209>.
 - [35] Y. Jia, H. He, Y. Geng, B. Huang, H. Peng, High through-plane thermal conductivity of polymer based product with vertical alignment of graphite flakes achieved via 3D printing, *Compos. Sci. Technol.* 145 (2017) 55–61.
 - [36] S. Yu, Y.H. Hwang, J.Y. Hwang, S.H. Hong, Analytical study on the 3D-printed structure and mechanical properties of basalt fiber-reinforced PLA composites using X-ray microscopy, *Compos. Sci. Technol.* 175 (2019) 18–27, <https://doi.org/10.1016/j.compscitech.2019.03.005>.